Journal of
Marine Science and Engineering

MDPI

Article

Underwater Wireless Sensor Network-Based Localization Method under Mixed Line-of-Sight/Non-Line-of-Sight Conditions

Ying Liu [1], Yingmin Wang [1], Cheng Chen [1,*] and Chenxi Liu [2]

[1] School of Marine Science and Technology, Northwestern Polytechnical University, Xi'an 710072, China; liuyouzi@mail.nwpu.edu.cn (Y.L.)
[2] School of Electronics and Information, Northwestern Polytechnical University, Xi'an 710072, China; liu_chenxi@mail.nwpu.edu.cn
* Correspondence: chen.cheng@nwpu.edu.cn; Tel.: +86-187-9276-6645

Abstract: Source localization in underwater sensor networks (UWSNs) presents complex challenges due to sensor nodes drift caused by ocean currents, non-line-of-sight (NLOS) propagation resulting from underwater multipath effects, and environmental noise. This paper proposes a practical and innovative algebraic solution based on the time difference of arrival (TDOA) for source localization in shallow seas. The proposed solution effectively addresses the issues arising from sensor position errors and multipath effects by incorporating the sea-surface reflection non-line-of-sight (SNLOS) link and optimizing the algorithm, thereby significantly improving positioning accuracy. The core concept of the method involves utilizing the weighted least squares algorithm to obtain an initial estimate of the source position, followed by direct estimation of the bias and subsequent refinement of the solution. In contrast to traditional closed-form solutions, this method avoids the introduction of intermediate parameters and directly handles the estimated bias from the previous step. Even when only considering the line-of-sight (LOS) link, the proposed solution achieves precise localization with a minimal number of sensors. Theoretical analysis demonstrates that the solution can achieve the Cramér–Rao lower bound (CRLB) accuracy under low noise conditions, and simulation results validate the superior performance of the proposed solution.

Keywords: underwater sensor networks; Cramér–Rao lower bound; non-line of sight; sea-surface reflection; line of sight; time difference of arrival

Citation: Liu, Y.; Wang, Y.; Chen, C.; Liu, C. Underwater Wireless Sensor Network-Based Localization Method under Mixed Line-of-Sight/Non-Line-of-Sight Conditions. *J. Mar. Sci. Eng.* **2023**, *11*, 1642. https://doi.org/10.3390/jmse11091642

Academic Editor: Christos Tsabaris

Received: 11 July 2023
Revised: 19 August 2023
Accepted: 21 August 2023
Published: 23 August 2023

1. Introduction

Underwater sensor networks (UWSNs) play a vital role in various fields, such as marine environment monitoring, underwater resource exploration, and natural disaster prevention and recovery [1–4]. One crucial task in UWSNs is underwater acoustic localization, which involves estimating the position of an underwater signal source based on measurements received by the network. However, the propagation of sound signals in water is influenced by several factors, including multipath propagation, signal attenuation, and ambient noise. Underwater source localization encounters significant challenges. Therefore, it is imperative to develop effective and robust algorithms for source localization in UWSNs.

Offering a comprehensive survey, Reference [5] reviews localization techniques for UWSNs. The foundational concepts are elucidated, covering key assumptions and range measurement methodologies. The work categorizes UWSN architectures based on node mobility into stationary, mobile, and hybrid networks, contrasting centralized and distributed localization approaches. Specific techniques like hyperbola-based and motion-aware self-localization are highlighted. From an algorithmic lens, localization algorithms are bifurcated into range-based methods such as Time Difference of Arrival (TDOA) [6,7],

Time of Arrival (TOA) [8,9], angle of arrival (AOA), and Received Signal Strength Indicator (RSSI), and range-free techniques including hop count and area-based techniques. Through practical examples, [5] provides an insightful comparison of the relative merits and limitations of these algorithms.

In UWSNs, TOA necessitates highly synchronized clocks between transmitters and receivers to ensure accurate measurements, whereas TDOA is less affected by clock synchronization. Achieving accurate clock synchronization is challenging in the underwater environment due to long signal propagation delays. Consequently, TDOA-based methods are often more effective than TOA-based approaches. However, traditional TDOA methods typically assume ideal LOS propagation, neglecting the impact of multipath effects. In harsh underwater environments, particularly in shallow seas, underwater acoustic channels often consist of multiple NLOS links. Another significant challenge is the movement or drift caused by ocean currents, which leads to inaccuracies in the positions of sensor nodes within the UWSN.

To tackle these challenges, we present a TDOA-based algebraic solution suitable for shallow seas. This method accurately locates the source in the presence of sensor node position errors by utilizing LOS and the sea-surface reflection non-line-of-sight (SNLOS) links. Firstly, we differentiate between the SNLOS links and the LOS links by classifying and processing underwater multipath signals. We then exploit the sea surface reflection properties to determine the position of the virtual sensor node associated with the SNLOS link. Taking into account potential TDOA measurement errors and sensor position inaccuracies, we incorporate measurement noise and sensor position noise to formulate a weighted coefficient matrix. Using the weighted least squares algorithm, we derive an initial estimate of the unknown source position. Subsequently, we compute the estimated deviation and refine the initial estimate to produce the final result.

The key contributions of this paper can be summarized as follows:

- Proposing a practical TDOA-based algebraic solution for underwater source localization in shallow seas, which addresses the challenges arising from sensor position errors and multipath effects;
- Exploiting the SNLOS link to introduce virtual sensors, providing additional TDOA measurement information;
- Employing the weighted least squares method to obtain an initial estimate of the source position, followed by direct estimation and correction of bias to refine the solution;
- Avoiding the introduction of intermediate parameters, allowing precise localization using only four sensors even when only the LOS link is considered;
- Deriving the CRLB and providing theoretical analysis showing the proposed solution can achieve CRLB accuracy under low noise conditions.

The rest of the paper is organized as follows. Section 2 provides an overview of the related work in underwater acoustic localization. Section 3 describes the localization scenario and summarizes the TDOA measurement model. Section 4 presents an algebraic solution for localization in the presence of LOS and NLOS links. The evaluation of the CRLB for this problem is discussed in Section 5, and theoretical analysis is provided to demonstrate that the proposed solution can achieve CRLB accuracy under specific conditions. Section 6 illustrates the performance of the proposed methods through simulations. Finally, Section 7 concludes the paper.

In this paper, bold lowercase letters represent vectors, while bold uppercase letters denote matrices. $\|\boldsymbol{\alpha}\|$ represents the l_2-norm of a vector. $\alpha(i)$ is the i-th element of vector $\boldsymbol{\alpha}$. $\mathrm{A}(:, j)$ represents the j-th column of matrix $\mathbf{A}$. $\boldsymbol{\alpha}^{\boldsymbol{o}}$ indicates the true value of its noisy counterpart. $\mathbf{0}_{\mathrm{N}}$ and $\mathbf{0}_{M\times N}$ represent zero vectors and matrices of appropriate size, respectively. All vectors are column vectors in this paper unless otherwise specified.

2. Related Work

The TDOA-based positioning method is a well-established technique in the field of passive localization. It involves estimating the position of a signal source by measuring the differences in arrival times of the signal at multiple receivers. Numerous TDOA algorithms have been developed and can be broadly categorized as either iterative methods [10–12] or non-iterative methods [13,14]. Iterative methods typically require accurate initial solution guesses and more computational resources. In contrast, non-iterative methods aim to directly estimate the position using analytical or closed-form solutions, eliminating the need for iterative refinement. Consequently, these methods significantly reduce algorithm complexity and enhance computational efficiency. One classic non-iterative approach is the two-step WLS method based on TDOA, introduced in [10], while an iterative method utilizing maximum likelihood estimation (MLE) was developed in [13]. The latter employs the semidefinite programming (SDP) technique to transform the non-convex problem into a convex optimization problem, enabling an iterative solution.

However, these studies rely heavily on the stability of the LOS link of the direct signal path. Recently, literature has emerged focusing on source localization in environments with NLOS links [14–19]. In [14], a method based on weighted least squares is proposed to solve the problem of TDOA-based localization in mixed LOS/NLOS environments. To effectively mitigate NLOS errors in TDOA systems, ref. [15] developed an SDP method with constraints. Furthermore, in a mixed LOS/NLOS environment, the positioning performance of TOA and TDOA within a cellular communication system was analyzed and compared in [16]. For precise localization in a TDOA-based indoor target positioning system and to combat NLOS link interference, a combined weighted method was proposed in [17]. The TDOA-based source localization problem under NLOS conditions is transformed into a robust least squares problem in [18], and two convex relaxation methods are proposed to solve this problem. In [19], a method for sensor selection in wireless sensor networks (WSNs) under NLOS conditions is presented.

However, direct application of the aforementioned methods to the underwater environment is hindered by various factors, including limited communication range, multipath effects, and the absence of global positioning systems like GPS. In the field of underwater passive localization, a method based on frequency diversity was proposed in [20] for multipath estimation. The algorithm simplifies the problem by representing all NLOS links as an equivalent NLOS link, and employs the differential evolution algorithm to tackle it. We proposed a closed-form solution in [21] for underwater acoustic localization that exploits multipath effects and corrects sensor position errors by introducing a single calibration source with a precisely known position.

The complexities of localization within UWSNs are delved into in [22], introducing both distance-based and angle-based schemes. By estimating inter-node distances or angles, node locations can be determined, and the average localization errors can be computed over multiple iterations. Simulations demonstrate that these methods prioritize energy efficiency and substantially decrease the average estimation errors, establishing a new standard for underwater data collection. In [23], a range difference-based source localization algorithm was developed for NLOS conditions in UWSN. The source localization problem is transformed into a generalized trust region subproblem to obtain an initial estimate, which is then iteratively refined to obtain the final estimate of the source localization. A closed least squares source location algorithm based on the angle of arrival (AOA) suitable for the shallow water multipath environment was presented in [18]. This method utilizes LOS and surface-reflected NLOS information to locate a drifted node. In [24], an efficient method for classifying LOS and NLOS links in underwater acoustic localization was proposed.

This paper builds on our previous work published in [21]. We improved the localization algorithm in [21] by considering LOS and SNLOS propagation in shallow seas. Our solution in this paper eliminates the need for a calibration source and achieves accurate source localization, even in the presence of uncertain sensor positions. Importantly, it

minimizes the number of nodes required for underwater acoustic positioning by avoiding intermediate variables, even in scenarios with only LOS links.

3. Scenario and Measurement Model

In the shallow marine environment, sound waves emitted by an unknown source can reach receiving sensors through various paths, including LOS and NLOS links. The underwater acoustic signal is significantly affected by multipath propagation. Theoretically, sensors can detect signals from numerous links, but in practice, signal energy loss is significant due to multiple reflections and refractions in the sea. Only links with higher energy, such as the LOS and SNLOS propagation, can be detected. This paper focuses on scenarios where the received signal includes the SNLOS link and the LOS link.

Figure 1 depicts the source localization model. The unknown underwater source is denoted as $\boldsymbol{u}^o = [x, y, z]$, while the M sensor nodes are positioned at $\boldsymbol{s}_{i,1}^o = [x_i, y_i, z_i](i = 2, 3, \ldots, M)$. The virtual sensor positions, which correspond to the SNLOS link, are mirror images of the sensor positions relative to the sea surface and are located at $\boldsymbol{s}_{i,2}^o = [x_i, y_i, -z_i](i = 2, 3, \ldots, M)$. For the purposes of TDOA measurement, $\boldsymbol{s}_1^o = [x_1, y_1, z_1]$ is designated as the reference node, and only its LOS link is taken into account.

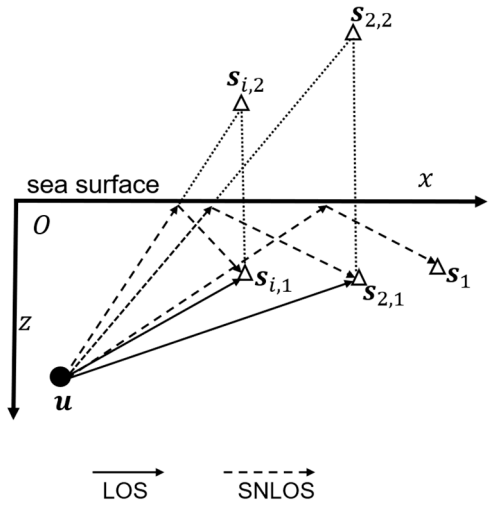

Figure 1. Underwater source localization model using LOS and SNLOS.

For simplicity, we assume a constant signal propagation speed, denoted as c. We have the measurements

$$r_{i1,l} = cT_{i1,l} = r_{i1,l}^o + n_{i1,l}, i = 2, 3, \ldots, M; l = 1, 2, \tag{1}$$

where $T_{i1,l}$ denotes the TDOA measured between the sensor pair i and 1 along path l. $r_{i1,l}$ is referred to as the range difference of arrival (RDOA) with noise $n_{i1,l}$.

In this paper, TDOA and RDOA are used interchangeably due to their equivalence. n_{i1} is the noise in RDOA measurements. $r_{i1,l}^o$ represents the true RDOA, and we have

$$r_{i1,l}^o = r_{i,l}^o - r_1^o = \left\| \boldsymbol{u}^o - \boldsymbol{s}_{i,l}^o \right\| - \| \boldsymbol{u}^o - \boldsymbol{s}_1^o \|, \tag{2}$$

where $\|\Delta\|$ indicates the $\updownarrow_2$ norm of Δ. By gathering all $M-1$ measurements together in matrix form, we obtain

$$\boldsymbol{r} = \boldsymbol{r^o} + \boldsymbol{n}, \tag{3}$$

where $\boldsymbol{r^o} = \left[r_{21,1}^o, r_{21,2}^o, \ldots, r_{M1,2}^o \right]$ and $\boldsymbol{n}$ is assumed to be a zero-mean Gaussian random vector with a covariance matrix $\mathbf{Q_n}$.

The true positions of the sensors, $s_{i,l}^{o}$, are often unknown, particularly when the underwater sensor nodes drift with the ocean current. In this study, the available sensor positions, $s_{i,l}$, are related to the true positions by

$$\boldsymbol{s} = \boldsymbol{s^o} + \Delta \boldsymbol{s}, \tag{4}$$

where $\boldsymbol{s} = \left[\boldsymbol{s}_1^T, \boldsymbol{s}_{2,l}^T, \ldots, \boldsymbol{s}_{M,l}^T\right]$ and $\boldsymbol{s^o} = \left[\boldsymbol{s}_{1,l}^{o\ T}, \boldsymbol{s}_{2,l}^{o\ T}, \ldots, \boldsymbol{s}_{M,l}^{o\ T}\right]$. $\Delta \boldsymbol{s}$ denotes the position error in $\boldsymbol{s}$, which is modeled as a zero-mean Gaussian random vector with a covariance matrix $\mathbf{Q_s}$.

4. The Proposed Algebraic Localization Algorithm

In this section, we propose a closed-form solution for the underwater localization problem in the presence of sensor position errors. Our solution is divided into two stages. Firstly, the virtual sensors associated with the SNLOS link are determined. Following that, the nonlinear equation is transformed into a pseudo-linear format and then solved. By introducing a polynomial equation, the range difference parameter and the source position parameter are separated, providing an initial estimate for the unknown source. In the second stage, the source position estimate is refined by calculating the error term, leveraging the initial solution from the first stage.

Stage 1: Initial estimation of the underwater source position.

In real-world oceanic conditions, both TDOA measurements and sensor positions are susceptible to errors, primarily due to the non-uniform nature of the propagation medium and the effects of ocean currents. Consequently, we initially incorporated the noise associated with TDOA measurements and the inaccuracies in sensor positions. Utilizing these, we formulated a weighted coefficient matrix, which facilitates a more precise preliminary estimation of the target's location. This estimation was derived using the weighted least squares method.

Rewriting (2), squaring both sides, and simplifying yield, we obtain

$$r_{i1,l}^{o\ 2} + 2r_{i1,l}^{o} r_1^{o} = \boldsymbol{s}_{i,l}^{o\ T}\boldsymbol{s}_{i,l}^{o} - \boldsymbol{s}_1^{o T}\boldsymbol{s}_1^{o} - 2\left(\boldsymbol{s}_{i,l}^{o} - \boldsymbol{s}_1^{o}\right)^T \boldsymbol{u}^{o}. \tag{5}$$

Substituting the $r_{i1,l}^{o}$ by $r_{i1,l}^{o} = r_{i1,l} - n_{i1,l}$ and $\boldsymbol{s}_{i,l}^{o}$ by $\boldsymbol{s}_{i,l}^{o} = \boldsymbol{s}_{i,l} - \Delta \boldsymbol{s}_{i,l}$, we have

$$r_{i1,l}{}^2 + \boldsymbol{s}_1{}^T\boldsymbol{s}_1 - \boldsymbol{s}_{i,l}{}^T\boldsymbol{s}_{i,l} + 2\left(\boldsymbol{s}_{i,l} - \boldsymbol{s}_1\right)^T \boldsymbol{u}^{o} + 2r_{i1,l} r_1^{o} = \epsilon_{i,l}, \tag{6}$$

where

$$\epsilon_{i,l} = 2r_{i,l}^{o} n_{i1,l} - 2\left(\boldsymbol{u}^{o} - \boldsymbol{s}_1\right)^T \Delta \boldsymbol{s}_1 + 2\left(\boldsymbol{u}^{o} - \boldsymbol{s}_{i,l}\right)^T \Delta \boldsymbol{s}_{i,l}, \tag{7}$$

where the second-order noise terms are ignored.

Let us define

$$\boldsymbol{h}_1 = \begin{bmatrix} r_{21,1}{}^2 + \boldsymbol{s}_1{}^T\boldsymbol{s}_1 - \boldsymbol{s}_{2,1}{}^T\boldsymbol{s}_{2,1} \\ r_{21,2}{}^2 + \boldsymbol{s}_1{}^T\boldsymbol{s}_1 - \boldsymbol{s}_{2,2}{}^T\boldsymbol{s}_{2,2} \\ \vdots \\ r_{M1,2}{}^2 + \boldsymbol{s}_1{}^T\boldsymbol{s}_1 - \boldsymbol{s}_{M,2}{}^T\boldsymbol{s}_{M,2} \end{bmatrix}, \tag{8}$$

$$\boldsymbol{G}_1 = \begin{bmatrix} 2\left(\boldsymbol{s}_1 - \boldsymbol{s}_{2,1}\right)^T \\ 2\left(\boldsymbol{s}_1 - \boldsymbol{s}_{2,2}\right)^T \\ \vdots \\ 2\left(\boldsymbol{s}_1 - \boldsymbol{s}_{M,2}\right)^T \end{bmatrix}, \tag{9}$$

$$\boldsymbol{\epsilon} = [\epsilon_{2,1}, \epsilon_{2,2}, \ldots, \epsilon_{M,2}]. \tag{10}$$

The equation error vector $\boldsymbol{\epsilon}$ can be rewritten as

$$\boldsymbol{\epsilon} = \boldsymbol{P}_1 \boldsymbol{n} + \boldsymbol{F}_1 \Delta \boldsymbol{s}, \tag{11}$$

where

$$\boldsymbol{P}_1 = 2\text{diag}\left\{\left[r_{2,1}^o, r_{2,2}^o, \ldots, r_{M,2}^o\right]\right\}, \tag{12}$$

$$\boldsymbol{F}_1 = \begin{bmatrix} -2(\boldsymbol{u}^o - \boldsymbol{s}_1)^T & 2(\boldsymbol{u}^o - \boldsymbol{s}_{2,1})^T & \cdots & \boldsymbol{0} \\ \vdots & \vdots & \ddots & \vdots \\ -2(\boldsymbol{u}^o - \boldsymbol{s}_1)^T & \boldsymbol{0} & \cdots & 2(\boldsymbol{u}^o - \boldsymbol{s}_{M,2})^T \end{bmatrix} \tag{13}$$

and $\text{diag}\{\boldsymbol{\alpha}\}$ is a diagonal matrix with the elements of $\boldsymbol{\alpha}$ as the diagonal.

Expressing (6) in matrix form yields

$$\boldsymbol{\epsilon} = \boldsymbol{h}_1 - \boldsymbol{G}_1\boldsymbol{u}^o + 2\boldsymbol{r}r_1^o. \tag{14}$$

By applying weighted least squares (WLS), we obtain the solution to (14) as follows:

$$\boldsymbol{u}_1 = \left(\boldsymbol{G}_1^T\boldsymbol{W}_1\boldsymbol{G}_1\right)^{-1}\boldsymbol{G}_1^T\boldsymbol{W}_1(\boldsymbol{h}_1 + 2\boldsymbol{r}r_1^o), \tag{15}$$

where the weighting matrix is $\boldsymbol{W}_1$ expressed as

$$\boldsymbol{W}_1 = \mathbb{E}\left[\boldsymbol{\epsilon}\boldsymbol{\epsilon}^T\right]^{-1} = \left(\boldsymbol{P}_1\boldsymbol{Q}_n\boldsymbol{P}_1^T + \boldsymbol{F}_1\boldsymbol{Q}_s\boldsymbol{F}_1^T\right)^{-1}, \tag{16}$$

where $\mathbb{E}[\boldsymbol{\alpha}]$ represents the expectation of $\boldsymbol{\alpha}$.

For simplicity, we can represent

$$\boldsymbol{\xi} = \left(\boldsymbol{G}_1^T\boldsymbol{W}_1^{-1}\boldsymbol{G}_1\right)^{-1}\boldsymbol{G}_1^T\boldsymbol{W}_1^{-1}\boldsymbol{h}_1, \tag{17}$$

$$\boldsymbol{\kappa} = 2\left(\boldsymbol{G}_1^T\boldsymbol{W}_1^{-1}\boldsymbol{G}_1\right)^{-1}\boldsymbol{G}_1^T\boldsymbol{W}_1^{-1}\boldsymbol{r}. \tag{18}$$

Hence,

$$\boldsymbol{u}_1 = \boldsymbol{\xi} + \boldsymbol{\kappa}r_1^o. \tag{19}$$

By squaring both sides of $r_1^o = \left\|\boldsymbol{s}_1^o - \boldsymbol{u}\right\|$ and substituting it into (19), we can simplify it to

$$\left(\|\boldsymbol{\kappa}\|^2 - 1\right)r_1^{o2} + 2\left(\boldsymbol{\xi} - \boldsymbol{s}_1^o\right)^T\boldsymbol{\kappa}r_1^o + \|\boldsymbol{\xi} - \boldsymbol{s}_1^o\|^2 = 0. \tag{20}$$

After computing r_1^o using Equation (20), substituting it into Equation (19) yields the solution for $\boldsymbol{u}_1$.

Stage 2: Estimation of the bias term:

This stage aims to refine the sound source estimation from the prior step, thereby enhancing the overall precision of localization. In this phase, we account for the target position error and formulate a new equation. Leveraging the weighted least squares algorithm, we ascertain this error. Utilizing this identified error, we refine the preliminary estimated position acquired in the initial phase, yielding a more accurate final outcome.

By defining the estimation error as $\Delta\boldsymbol{u}_1 = \boldsymbol{u}_1 - \boldsymbol{u}^o$ and considering the first-order Taylor-series expansion, r_1^o can be expressed as

$$r_1^o = \|\boldsymbol{u}_1 - \boldsymbol{s}_1\| - \boldsymbol{\rho}_{\boldsymbol{u}_1,\boldsymbol{s}_1}^T\Delta\boldsymbol{u}_1 + \boldsymbol{\rho}_{\boldsymbol{u}_1,\boldsymbol{s}_1}^T\Delta\boldsymbol{s}_{i,l}, \tag{21}$$

where the second-order noise term is neglected, and $\boldsymbol{\rho}_{\boldsymbol{\alpha},\boldsymbol{\beta}}^T = (\boldsymbol{\alpha} - \boldsymbol{\beta})^T / \|\boldsymbol{\alpha} - \boldsymbol{\beta}\|$.

Substituting (21) into the RDOA measurement Equation (5) and incorporating the noise of the measured value, we obtain

$$\begin{aligned} e_{i,l} \quad &= {r_{i1,l}}^2 + {\boldsymbol{s}_1}^T\boldsymbol{s}_1 - {\boldsymbol{s}_{i,l}}^T\boldsymbol{s}_{i,l} + 2(\boldsymbol{s}_{i,l} - \boldsymbol{s}_1)^T\boldsymbol{u}_1 \\ &+ 2r_{i1,l}\|\boldsymbol{u}_1 - \boldsymbol{s}_1\| - 2\left[(\boldsymbol{s}_{i,l} - \boldsymbol{s}_1)^T + r_{i1,l}\boldsymbol{\rho}_{\boldsymbol{u}_1,\boldsymbol{s}_1}^T\right]\Delta u', \end{aligned} \tag{22}$$

where

$$e_{i,l} = 2\|\boldsymbol{u}_1 - \boldsymbol{s}_{i,l}\|n_{i1,l} - 2\left[\left(\boldsymbol{u}_1 - \boldsymbol{s}_1\right)^T + r_{i1,l}\rho_{\boldsymbol{u}_1,\boldsymbol{s}_1}^T\right]\Delta\boldsymbol{s}_1 + 2\left[\left(\boldsymbol{u}_1 - \boldsymbol{s}_{i,l}\right)^T\right]\Delta\boldsymbol{s}_{i,l}. \tag{23}$$

Forming a matrix by collecting Equation (22) for all $M-1$ RDOA measurements, we have

$$\boldsymbol{e} = \boldsymbol{h}_2 - \boldsymbol{G}_2\Delta\boldsymbol{u}_1, \tag{24}$$

where

$$\boldsymbol{h}_2 = \begin{bmatrix} {r_{21,1}}^2 + {\boldsymbol{s}_1}^T\boldsymbol{s}_1 - {\boldsymbol{s}_{2,1}}^T\boldsymbol{s}_{2,1} + 2\left(\boldsymbol{s}_{2,1} - \boldsymbol{s}_1\right)^T\boldsymbol{u}_1 + 2r_{21,1}\|\boldsymbol{u}_1 - \boldsymbol{s}_1\| \\ {r_{22,1}}^2 + {\boldsymbol{s}_1}^T\boldsymbol{s}_1 - {\boldsymbol{s}_{2,2}}^T\boldsymbol{s}_{2,2} + 2\left(\boldsymbol{s}_{2,2} - \boldsymbol{s}_1\right)^T\boldsymbol{u}_1 + 2r_{21,2}\|\boldsymbol{u}_1 - \boldsymbol{s}_1\| \\ \vdots \\ {r_{M1,2}}^2 + {\boldsymbol{s}_1}^T\boldsymbol{s}_1 - {\boldsymbol{s}_{M,2}}^T\boldsymbol{s}_{M,2} + 2\left(\boldsymbol{s}_{M,2} - \boldsymbol{s}_1\right)^T\boldsymbol{u}_1 + 2r_{M1,2}\|\boldsymbol{u}_1 - \boldsymbol{s}_1\| \end{bmatrix}, \tag{25}$$

$$\boldsymbol{G}_2 = 2\begin{bmatrix} \left(\boldsymbol{s}_{2,1} - \boldsymbol{s}_1\right)^T + 2r_{21,1}\rho_{\boldsymbol{u}_1,\boldsymbol{s}_1}^T \\ \left(\boldsymbol{s}_{2,2} - \boldsymbol{s}_1\right)^T + r_{21,2}\rho_{\boldsymbol{u}_1,\boldsymbol{s}_1}^T \\ \vdots \\ \left(\boldsymbol{s}_{M,2} - \boldsymbol{s}_1\right)^T + r_{M1,2}\rho_{\boldsymbol{u}_1,\boldsymbol{s}_1}^T \end{bmatrix}. \tag{26}$$

The error vector $\boldsymbol{e}$ can be expressed as

$$\boldsymbol{e} = \boldsymbol{P}_2\boldsymbol{n} + \boldsymbol{F}_2\Delta\boldsymbol{s}, \tag{27}$$

where

$$\boldsymbol{P}_2 = 2\mathrm{diag}\{[\|\boldsymbol{u}_1 - \boldsymbol{s}_{2,1}\|, \|\boldsymbol{u}_1 - \boldsymbol{s}_{2,2}\|, \ldots, \|\boldsymbol{u}_1 - \boldsymbol{s}_{M,2}\|]\}, \tag{28}$$

$$\boldsymbol{F}_2 = 2\begin{bmatrix} -\left(\boldsymbol{u}_1 - \boldsymbol{s}_1\right)^T - r_{21,1}\rho_{\boldsymbol{u}_1,\boldsymbol{s}_1}^T & \left(\boldsymbol{u}_1 - \boldsymbol{s}_{2,1}\right)^T & \cdots & \boldsymbol{0} \\ \vdots & \vdots & \ddots & \vdots \\ -\left(\boldsymbol{u}_1 - \boldsymbol{s}_1\right)^T - r_{M1,2}\rho_{\boldsymbol{u}_1,\boldsymbol{s}_1}^T & \boldsymbol{0} & \cdots & \left(\boldsymbol{u}_1 - \boldsymbol{s}_{M,2}\right)^T \end{bmatrix}. \tag{29}$$

The solution to Equation (24) using WLS is given by

$$\Delta\overline{\boldsymbol{u}_1} = \left(\boldsymbol{G}_2^T\boldsymbol{W}_2\boldsymbol{G}_2\right)^{-1}\boldsymbol{G}_2^T\boldsymbol{W}_2^{-1}\boldsymbol{h}_2. \tag{30}$$

The weighting matrix $\boldsymbol{W}_2$ is given by

$$\boldsymbol{W}_2 = \mathbb{E}\left[\boldsymbol{e}\boldsymbol{e}^T\right]^{-1} = \left(\boldsymbol{P}_2\boldsymbol{Q}_n\boldsymbol{P}_2^T + \boldsymbol{F}_2\boldsymbol{Q}_s\boldsymbol{F}_2^T\right)^{-1}. \tag{31}$$

After calculating $\Delta\overline{\boldsymbol{u}}$ using (30), the final estimate for the unknown source position is

$$\boldsymbol{u}_2 = \boldsymbol{u}_1 - \Delta\overline{\boldsymbol{u}_1}. \tag{32}$$

5. CRLB and Performance Analysis

In this section, we derive the CRLB for the localization scenario illustrated in Figure 1 and analyze the performance of the proposed algebraic solution.

5.1. Derivation of CRLB

The CRLB establishes a stringent lower limit on the variance of an unbiased estimator. Essentially, it delineates the utmost level of accuracy achievable when estimating the position of the source based on the available measurements. The derivation of the CRLB relies on the utilization of the Fisher Information matrix (FIM), which serves to quantify the informational value encapsulated within the measurements pertaining to the position

of the unknown objective. Let us start by evaluating the probability density function (PDF) of the composite vector $\left[\boldsymbol{r}^T, \boldsymbol{s}^T\right]^T$,

$$\mathbb{P}(\boldsymbol{r}, \boldsymbol{s}; \boldsymbol{u}^o, \boldsymbol{s}^o) = K{\cdot}exp\left[-\frac{1}{2}(\boldsymbol{r}-\boldsymbol{r}^o)^T\boldsymbol{Q}_{\boldsymbol{n}}(\boldsymbol{r}-\boldsymbol{r}^o) - \frac{1}{2}(\boldsymbol{s}-\boldsymbol{s}^o)^T\boldsymbol{Q}_{\boldsymbol{s}}(\boldsymbol{s}-\boldsymbol{s}^o)\right], \tag{33}$$

where K represents a constant independent of the unknowns. The computation of the FIM can be expressed as follows:

$$\text{FIM} = \begin{bmatrix}\mathbf{X} & \mathbf{Y}\\ \mathbf{Y} & \mathbf{Z}\end{bmatrix}, \tag{34}$$

where

$$\mathbf{X} = -\mathbb{E}\left[\frac{\partial \ln \mathbb{P}}{\partial \boldsymbol{u}^o \partial \boldsymbol{u}^{oT}}\right] = \left(\frac{\partial \boldsymbol{r}^o}{\partial \boldsymbol{u}^o}\right)^T \boldsymbol{Q}_{\boldsymbol{n}}\left(\frac{\partial \boldsymbol{r}^o}{\partial \boldsymbol{u}^o}\right), \tag{35}$$

$$\mathbf{Y} = -\mathbb{E}\left[\frac{\partial \ln \mathbb{P}}{\partial \boldsymbol{u}^o \partial \boldsymbol{s}^{oT}}\right] = \left(\frac{\partial \boldsymbol{r}^o}{\partial \boldsymbol{u}^o}\right)^T \boldsymbol{Q}_{\boldsymbol{n}}\left(\frac{\partial \boldsymbol{r}^o}{\partial \boldsymbol{s}^o}\right), \tag{36}$$

$$\mathbf{Z} = -\mathbb{E}\left[\frac{\partial \ln \mathbb{P}}{\partial \boldsymbol{s}^o \partial \boldsymbol{s}^{oT}}\right] = \left(\frac{\partial \boldsymbol{r}^o}{\partial \boldsymbol{s}^o}\right)^T \boldsymbol{Q}_{\boldsymbol{n}}\left(\frac{\partial \boldsymbol{r}^o}{\partial \boldsymbol{s}^o}\right) + \boldsymbol{Q}_{\boldsymbol{s}}. \tag{37}$$

Next, we proceed to evaluate the partial derivatives $\partial \boldsymbol{r}^o / \partial \boldsymbol{u}^o$ and $\partial \boldsymbol{r}^o / \partial \boldsymbol{u}^o$.

$$\frac{\partial \boldsymbol{r}^o}{\partial \boldsymbol{u}^o} = \begin{bmatrix}\boldsymbol{\rho}_{\boldsymbol{u}^o,\boldsymbol{s}_{2,1}}^T - \boldsymbol{\rho}_{\boldsymbol{u}^o,\boldsymbol{s}_1}^T\\ \boldsymbol{\rho}_{\boldsymbol{u}^o,\boldsymbol{s}_{2,2}}^T - \boldsymbol{\rho}_{\boldsymbol{u}^o,\boldsymbol{s}_1}^T\\ \vdots\\ \boldsymbol{\rho}_{\boldsymbol{u}^o,\boldsymbol{s}_{M,2}}^T - \boldsymbol{\rho}_{\boldsymbol{u}^o,\boldsymbol{s}_1}^T\end{bmatrix}, \tag{38}$$

$$\frac{\partial \boldsymbol{r}^o}{\partial \boldsymbol{s}^o} = \begin{bmatrix}\boldsymbol{\rho}_{\boldsymbol{u}^o,\boldsymbol{s}_1}^T & -\boldsymbol{\rho}_{\boldsymbol{u}^o,\boldsymbol{s}_{2,1}}^T & \mathbf{0} & \mathbf{0} & \mathbf{0}\\ \boldsymbol{\rho}_{\boldsymbol{u}^o,\boldsymbol{s}_1}^T & \mathbf{0} & -\boldsymbol{\rho}_{\boldsymbol{u}^o,\boldsymbol{s}_{2,2}}^T & \cdots & \mathbf{0}\\ \vdots & \vdots & \vdots & \ddots & \vdots\\ \boldsymbol{\rho}_{\boldsymbol{u}^o,\boldsymbol{s}_1}^T & \mathbf{0} & \mathbf{0} & \cdots & -\boldsymbol{\rho}_{\boldsymbol{u}^o,\boldsymbol{s}_{M,2}}^T\end{bmatrix}. \tag{39}$$

By invoking the partitioned matrix inversion formula [25], we obtain:

$$CRLB(\boldsymbol{u}) = \text{FIM}^{-1} = \left(\mathbf{X} - \mathbf{Y}\mathbf{Z}^{-1}\mathbf{Y}^T\right)^{-1} = \mathbf{X}^{-1} + \mathbf{X}^{-1}\mathbf{Y}\left(\mathbf{Z} - \mathbf{Y}^T\mathbf{X}^{-1}\mathbf{Y}\right)^{-1}\mathbf{Y}^T\mathbf{X}^{-1}. \tag{40}$$

It is worth noting that $\mathbf{X}^{-1}$ is the CRLB of $\boldsymbol{u}$ when the source location is known exactly. The second term in (38) represents the increase in CRLB due to errors in the source positions. The trace of $CRLB(\boldsymbol{u})$ is the minimum possible source location MSE that any linear unbiased estimator can achieve.

To obtain intuitive insights, we perform simulations comparing the CRLB across four scenarios. Besides $CRLB(\boldsymbol{u})$ in (40) (denoted by CRLB-SNLOS-E), we considered a CRLB that accounts only for the SNLOS link, ignoring the sensor position errors (denoted by CRLB-SNLOS-NE). We also included two CRLBs: one with sensor error knowledge for the LOS link (denoted by CRLB-LOS-E) and one without such knowledge (denoted by CRLB-LOS-NE) for comparison. The true positions of the sensors are provided in Table 1. The RDOA measurements are generated by adding zero-mean white Gaussian noise to the true values. The noise covariance matrix is denoted as $\boldsymbol{Q}_{\boldsymbol{n}} = 0.5\boldsymbol{R}_{\boldsymbol{n}}$, where $\boldsymbol{R}_{\boldsymbol{n}}$ is a $3{\cdot}(2M-1) \times 3{\cdot}(2M-1)$ matrix with ${\sigma_n}^2$ in the diagonal and $0.5{\sigma_n}^2$ in all other elements, and ${\sigma_n}^2$ is fixed at 0.01. Similarly, the covariance matrix corresponding to the position errors of the sensor nodes is denoted as $\boldsymbol{Q}_{\boldsymbol{s}} = {\sigma_S}^2\boldsymbol{I}_{3{\cdot}(2M-1)\times 3{\cdot}(2M-1)}$.

Table 1. True sensor positions (in meters).

Sensor No.	1	2	3	4	5	6
x_i	238	−640	160	−314	560	890
y_i	−127	457	−200	85	−439	232
z_i	330	176	372	157	349	88

Figure 2 displays the CRLBs for the four cases with increasing noise power, where a stationary source $\boldsymbol{u^o} = [230, 500, -100]^T$ m is positioned near the sensors. In general, incorporating the SNLOS link decreases the CRLB by approximately 10 dB. This improvement is attributed to the introduction of virtual sensors, which enrich the TDOA measurements. The deviation in CRLBs between scenarios with and without sensor position errors becomes noticeable at ${\sigma_S}^2 = 0.1$, and their magnitude gradually amplifies with higher ${\sigma_S}^2$.

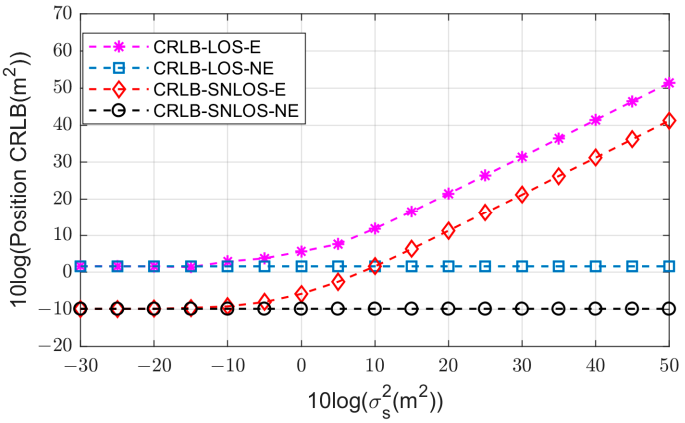

Figure 2. Comparisons of the CRLBs for a near stationary source.

Similarly, Figure 3 compares the CRLBs when the unknown source is positioned at $\boldsymbol{u^o} = [480, -1500, 1700]^T$, far from the sensor array. The overall trend observed closely resembles that in Figure 2. Notably, when the source is distant from the sensors, the CRLBs increase by roughly 10 dB compared to the case where the source is nearby. This is because TDOA-based positioning methods exhibit enhanced performance when the source is in close proximity to the sensors.

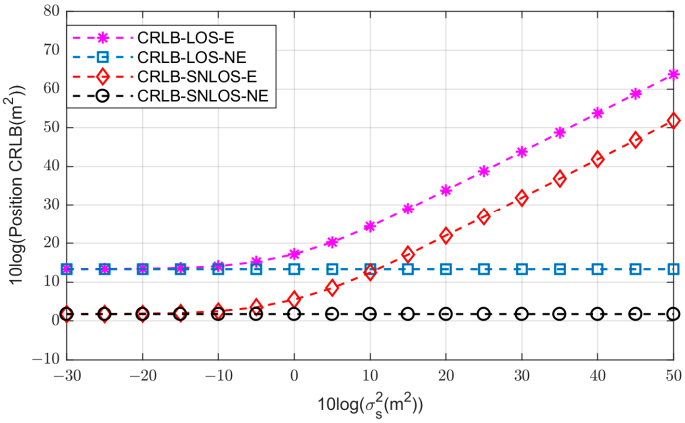

Figure 3. Comparisons of the CRLBs for a far stationary source.

5.2. Performance Analysis of the Proposed Algorithm

The study presented in this subsection is based on a first-order analysis, where the consideration of second and higher-order error terms is neglected. Therefore, the results

are valid only under the assumption that the RDOA noise and sensor position errors are sufficiently small.

By employing (30) and (32), the estimated error component $\Delta \boldsymbol{u}_2$ in the final source position estimate $\boldsymbol{u}_2$ can be expressed as

$$\Delta \boldsymbol{u}_2 = \left(\boldsymbol{G}_2^T \boldsymbol{W}_2 \boldsymbol{G}_2\right)^{-1} \boldsymbol{G}_2^T \boldsymbol{W}_2 (\boldsymbol{P}_2 \boldsymbol{n} + \boldsymbol{F}_2 \Delta \boldsymbol{s}). \tag{41}$$

To ensure the proposed solution remains unbiased, we compare the covariance matrix of $\boldsymbol{u}_2$ with the CRLB under the condition where the RDOA measurement noise and sensor errors are small. Hence, we have

$$\operatorname{cov}(\boldsymbol{u}_2) = \mathbb{E}\left[\Delta \boldsymbol{u}_2 \Delta \boldsymbol{u}_2^T\right] = \left[\boldsymbol{\Lambda}^T \boldsymbol{Q}_n^{-1} \boldsymbol{\Lambda} - \boldsymbol{\Lambda}^T \boldsymbol{Q}_n^{-1} \boldsymbol{\Gamma} \left(\boldsymbol{Q}_s^{-1} + \boldsymbol{\Gamma}^T \boldsymbol{Q}_n^{-1} \boldsymbol{\Gamma}\right)^{-1} \boldsymbol{\Gamma}^T \boldsymbol{Q}_n^{-1} \boldsymbol{\Lambda}\right]^{-1}, \tag{42}$$

where

$$\boldsymbol{\Lambda} = \boldsymbol{P}_2^{-1} \boldsymbol{G}_2, \tag{43}$$

$$\boldsymbol{\Gamma} = \boldsymbol{P}_2^{-1} \boldsymbol{F}_2. \tag{44}$$

After substituting $\boldsymbol{P}_2$ from (28) and $\boldsymbol{G}_2$ from (26) into (43), and simplifying the expression, we can derive

$$\boldsymbol{\Lambda} = \left[\frac{(\boldsymbol{u}^o - \boldsymbol{s}_{i,l})^T}{r_{i,l}^o} - \frac{(\boldsymbol{u}^o - \boldsymbol{s}_1)^T}{r_{i,l}^o} - \frac{r_{i1}}{r_{i,l}^o}\right] \times \begin{bmatrix} \mathbf{I}_{3\times 3} \\ \boldsymbol{\rho}_{\boldsymbol{u}^o, \boldsymbol{s}_1}^T \end{bmatrix}. \tag{45}$$

where the RDOA measurement noises are considerably smaller than the distance between the unknown source $\boldsymbol{u}^o$ and the sensor $\boldsymbol{s}_{i,l}^o$, that is

$$\frac{|n_{i1,l}|}{r_{i,l}^o} \approx 0, i = 2, 3, \ldots, M; l = 1, 2, \tag{46}$$

The $i-1$st row of $\boldsymbol{\Lambda}$ in (45) can be approximated as follows:

$$\boldsymbol{\Lambda}[i-1, :] \approx \left[\boldsymbol{\rho}_{\boldsymbol{u}^o, \boldsymbol{s}_{i,l}}^T - \frac{r_1^o}{r_{i,l}^o} \boldsymbol{\rho}_{\boldsymbol{u}^o, \boldsymbol{s}_1}^T - \left(1 - \frac{r_1^o}{r_{i,l}^o}\right)\right] \times \begin{bmatrix} \mathbf{I}_{3\times 3} \\ \boldsymbol{\rho}_{\boldsymbol{u}^o, \boldsymbol{s}_1}^T \end{bmatrix} = \boldsymbol{\rho}_{\boldsymbol{u}^o, \boldsymbol{s}_{i,l}}^T - \boldsymbol{\rho}_{\boldsymbol{u}^o, \boldsymbol{s}_1}^T. \tag{47}$$

When the 2-norm of the sensor position error vector, $\Delta \boldsymbol{s}$, is considerably smaller than the distance between the unknown source $\boldsymbol{u}^o$ and the sensor $\boldsymbol{s}_{i,l}^o$, this assumption can be expressed as

$$\frac{\left\|\Delta \boldsymbol{s}_{i,l}\right\|}{r_{i,l}^o} \approx 0, i = 2, 3, \ldots, M; l = 1, 2. \tag{48}$$

We can obtain

$$\boldsymbol{\rho}_{\boldsymbol{u}^o, \boldsymbol{s}_{i,l}}^T = \boldsymbol{\rho}_{\boldsymbol{u}^o, \boldsymbol{s}_{i,l}^o}^T, \tag{49}$$

and $\boldsymbol{\Lambda}$ can be approximated by

$$\boldsymbol{\Lambda} \approx \begin{bmatrix} \boldsymbol{\rho}_{\boldsymbol{u}^o, \boldsymbol{s}_{21}^o}^T - \boldsymbol{\rho}_{\boldsymbol{u}^o, \boldsymbol{s}_1^o}^T \\ \boldsymbol{\rho}_{\boldsymbol{u}^o, \boldsymbol{s}_{2,2}^o}^T - \boldsymbol{\rho}_{\boldsymbol{u}^o, \boldsymbol{s}_1^o}^T \\ \vdots \\ \boldsymbol{\rho}_{\boldsymbol{u}^o, \boldsymbol{s}_{M,2}^o}^T - \boldsymbol{\rho}_{\boldsymbol{u}^o, \boldsymbol{s}_1^o}^T \end{bmatrix}. \tag{50}$$

Similarly, by substituting (28) and (29) into (44), we obtain the following:

$$\mathbf{\Gamma}[i-1,:] = \left[-\left(1 - \frac{r_1^o}{r_{i,l}^o}\right)\boldsymbol{\rho}_{\boldsymbol{u}^o,\boldsymbol{s}_{i,l}}^T \quad -\frac{r_1^o}{r_{i,l}^o}\boldsymbol{\rho}_{\boldsymbol{u}^o,\boldsymbol{s}_{i,l}}^T \quad \mathbf{0} \quad \frac{\left(\boldsymbol{u}^o - \boldsymbol{s}_{i,l}^o\right)}{r_{i,l}^o} \right]. \tag{51}$$

Under the conditions of (46), (51) can be approximated as the following:

$$\mathbf{\Gamma} \approx \begin{bmatrix} \boldsymbol{\rho}_{\boldsymbol{u}^o,\boldsymbol{s}_1^o}^T & -\boldsymbol{\rho}_{\boldsymbol{u}^o,\boldsymbol{s}_{21}^o}^T & \mathbf{0} & \mathbf{0} & \mathbf{0} \\ \boldsymbol{\rho}_{\boldsymbol{u}^o,\boldsymbol{s}_1^o}^T & \mathbf{0} & -\boldsymbol{\rho}_{\boldsymbol{u}^o,\boldsymbol{s}_{2,2}^o}^T & \cdots & \mathbf{0} \\ \vdots & \vdots & \vdots & \ddots & \vdots \\ \boldsymbol{\rho}_{\boldsymbol{u}^o,\boldsymbol{s}_1^o}^T & \mathbf{0} & \mathbf{0} & \cdots & -\boldsymbol{\rho}_{\boldsymbol{u}^o,\boldsymbol{s}_{M,2}^o}^T \end{bmatrix}. \tag{52}$$

For comparison, we consider the $CRLB(\boldsymbol{u})$ from (35) as

$$CRLB(\boldsymbol{u}) = \left(\mathbf{X} - \mathbf{X}\mathbf{Z}^{-1}\mathbf{Y}^T\right)^{-1}. \tag{53}$$

A notable observation is that the $CRLB(\boldsymbol{u})$ and the covariance matrix $\mathrm{cov}(\boldsymbol{u}_2)$ share the same structural form. By substituting $\mathbf{X}$, $\mathbf{Y}$, and $\mathbf{Z}$ from (35) into (53) and comparing it with $\mathrm{cov}(\boldsymbol{u}_2)$, we obtain the following:

$$\mathbf{\Lambda} \approx \frac{\partial \boldsymbol{r}^o}{\partial \boldsymbol{u}^o}, \tag{54}$$

$$\mathbf{\Gamma} \approx \frac{\partial \boldsymbol{r}^o}{\partial \boldsymbol{s}^o}. \tag{55}$$

Hence, it can be concluded that the proposed solution achieves the CRLB accuracy when both (46) and (48) are satisfied.

6. Simulation Results

In this section, we conduct simulations to verify the performance of the proposed method and compare it with the CRLB and two existing similar methods. The first is the MP method (referred to as "MP-Solution"), which was developed for shallow water multipath environments, as described in [21]. By exploiting multipath effects in shallow seas and introducing a single calibration source, the method corrects sensor position errors and enhances localization performance. The other is the SDP method in [13], which is utilized as the initial solution for the iterative MLE approach (referred to as "SDP-MLE") and was devised to tackle sensor position inaccuracies in TDOA localization. It is important to note that the localization models used in these methods differ slightly from the model employed in this article. Further details regarding the model adjustments will be provided in subsequent simulation scenarios. The other simulation parameters are consistent with those in Section 3. Performance evaluation is based on the MSE criterion, defined as $MSE(\boldsymbol{u}) = \frac{1}{M}\sum_{k=1}^{M}\left\|\boldsymbol{u}^k - \boldsymbol{u}^o\right\|^2$, where M represents the number of Monte Carlo runs, and $\boldsymbol{u}^k$ corresponds to the estimate of the true value $\boldsymbol{u}^o$ in the k-th run. The number of ensemble runs is set to 5000.

6.1. The Impact of the Distance between Source and Sensor Nodes

In this simulation scenario, we consider six sensor nodes whose true positions are provided in Table 1. To ensure a meaningful comparison of algorithm performance, we standardize the positioning models across the three methods. Specifically, for the MP solution, only the sea surface reflection path is utilized. In the case of the SDP-MLE method, we introduce additional virtual sensor positions denoted by $\boldsymbol{s}_{i,2}^o = [x_i, y_i, -z_i](i = 2, 3, \ldots, M)$ to unify the localization model.

Figure 4 presents the performance comparison of different solutions for a near-stationary source located at $\boldsymbol{u^o} = [230, 500, -100]^T$ m as the noise power increases. The three solutions exhibit comparable performance in achieving CRLB accuracy when the noise level ${\sigma_S}^2$ is below 1. However, as the noise power grows, the proposed method consistently tracks the CRLB accurately and outperforms the other algorithms significantly. The SDP-MLE method begins to deviate from the CRLB at ${\sigma_S}^2 = 1$, while the MP solution deviates at ${\sigma_S}^2 = 10$.

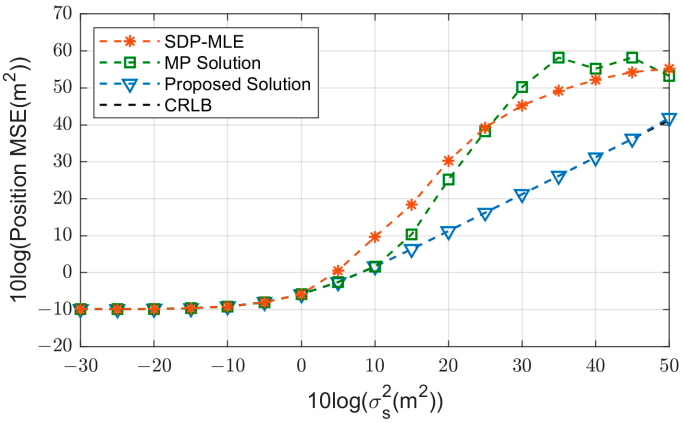

Figure 4. Comparisons of the MSE for a near stationary source.

The performance of the SDP-MLE method suffers due to approximation errors from truncating the second-order Taylor series, as described in [13]. On the other hand, the MP solution experiences performance deterioration because of the introduction of pseudo-linear equations, which makes it susceptible to the threshold effect and causes rapid deviation from the CRLB as the noise level rises.

Figure 5 illustrates the performance of the three estimators when the source is located at $\boldsymbol{u^o} = [230, 500, -100]^T$ m, far away from the sensor array. Similar to Figure 4, the proposed method maintains good adherence to the CRLB as the noise power increases, exhibiting superior performance compared to SDP-MLE and the MP solution.

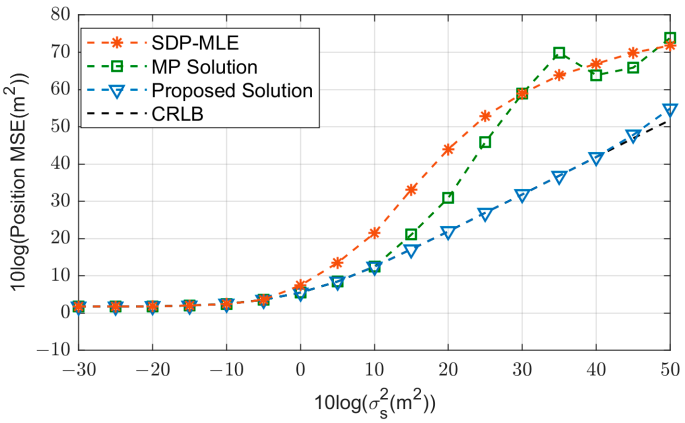

Figure 5. Comparisons of the MSE for a far stationary source.

Comparing Figure 5 to Figure 4, we observe that the accuracy of localization for a far source, about 10 dB, is generally lower than that for a nearby source. This can be attributed to the hyperbolic nature of TDOA measurements. As the distance between the source and the receiver sensors increases, the impact of measurement errors and uncertainties in TDOAs becomes more prominent, leading to a significant decrease in positioning accuracy.

6.2. The Impact of Using Only Four Sensor Nodes

We proceeded to evaluate the localization performance of the proposed solution using the minimum number of sensors. Specifically, we utilized only four receiving sensors, which satisfies the minimum requirement for 3D localization. These sensors were selected from the entries in Table 1. The model parameters matched the specifications in Figure 4, with the near source at $\boldsymbol{u^o} = [230, 500, -100]^T$.

Figure 6 plots the performance of the three methods as noise power increases using the SNLOS link. It is evident that the introduction of virtual sensors enables all three algorithms to achieve the CRLB when ${\sigma_S}^2 < 0.1$. However, in comparison to Figure 4, the SDP-MLE and MP solution begins to deviate from the CRLB earlier due to the reduced number of sensors. In contrast, the proposed solution continues to exhibit superior performance and closely follows the CRLB.

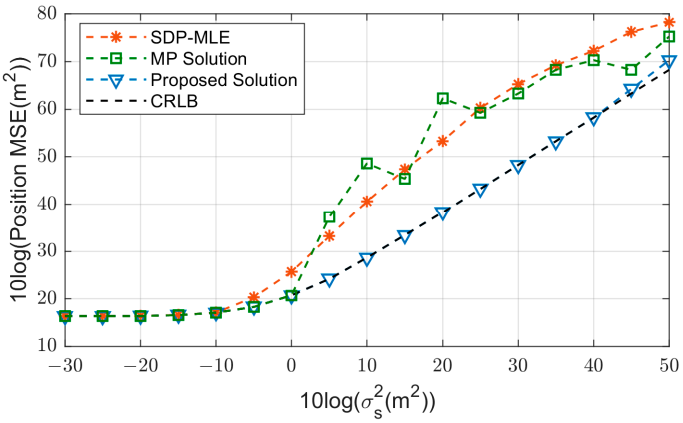

Figure 6. Comparisons of the MSE for 4 receiver sensors.

Figure 7 displays the results obtained when only the LOS links are considered. It is evident that the overall performance of the algorithms decreased. Specifically, the MP solution lost its point source positioning capability. This is because the MP solution heavily relies on leveraging the underwater multipath effect to enhance its positioning accuracy. However, its assumptions about the underwater environment are overly idealistic, and in practical scenarios, it is often challenging to receive a substantial number of multipath signals. When disregarding the multipath effect, the MP solution requires at least five sensors to be effective due to the introduction of intermediate parameters in the algorithm. On the other hand, SDP-MLE can still achieve the CRLB when the noise level is extremely low. Although the proposed solution starts deviating from the CRLB when ${\sigma_S}^2 > 10^3$, it remains capable of accurately and effectively locating the unknown source under moderate noise conditions.

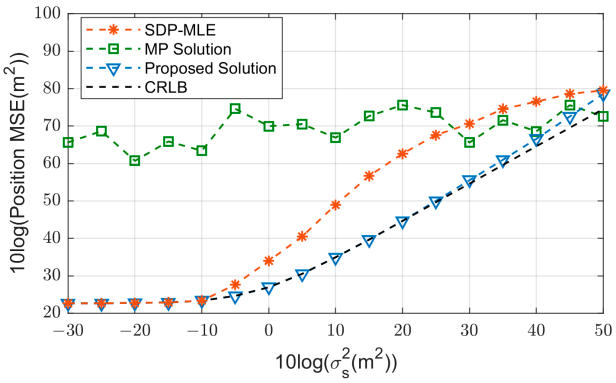

Figure 7. Comparisons of the MSE for 4 receiver sensors ignoring SNLOS.

Algebraic solutions have gained popularity due to their computational efficiency and ability to avoid getting trapped in local optima. Table 2 presents the processing times for the algorithms utilized in the simulation scenario depicted in Figure 4. The proposed closed-form solution exhibits a processing time that is 729.10 times lower than that of SDP-MLE and approximately comparable to the MP solution. In SDP-MLE, the semidefinite relaxed programming utilized for initialization accounts for 96.9% of the total computation time.

Table 2. Computation processing times.

Solution	Posed Solution	MP Solution	SDP-MLE
Time(s)	3.62	5.87	2639.7
Rel. Time	1	1.62	729.20

7. Conclusions

In this study, we introduced an innovative algebraic solution for underwater source localization in shallow seas, which addresses the challenges arising from sensor position errors and multipath effects. By exploiting LOS and SNLOS links, our method provides a robust approach to underwater acoustic localization. Theoretical analysis demonstrates that the proposed solution achieves CRLB accuracy when TDOA measurement noise and sensor position errors are sufficiently small. Simulation results illustrate that the proposed algorithm maintains higher positioning accuracy over a wider noise range compared to previous methods like MP and SDP-MLE, closely following the CRLB. Moreover, our closed-form solution is computationally more efficient than iterative localization algorithms. A comprehensive simulation comparison verifies the robustness and efficiency of the proposed solution, highlighting its potential for practical applications in underwater sensor networks.

Author Contributions: Conceptualization, Y.L. and C.L.; methodology, Y.L.; software, C.C.; validation, Y.L. and C.C.; formal analysis, Y.L.; investigation, Y.L. and C.C.; resources, Y.L.; data curation, C.C.; writing—original draft preparation, Y.L.; writing—review and editing, C.C. and Y.W.; visualization, C.C. and C.L.; supervision, C.C.; project administration, Y.W.; funding acquisition, Y.W. All authors have read and agreed to the published version of the manuscript.

Funding: This research was funded by the National Natural Science Foundation of China (Grant No. 51879221, Grant No. 52101389); the Natural Science Foundation of Shandong Province, China (Grant No. ZR201910220437); the Open Fund of State Key Laboratory of Acoustics (Grant No. SKLA202103); and Fundamental Research Funds for the Central Universities.

Institutional Review Board Statement: Not applicable.

Informed Consent Statement: Not applicable.

Data Availability Statement: Data associated with this research are available and can be obtained by contacting the corresponding author upon reasonable request.

Conflicts of Interest: The authors declare no conflict of interest. The funders had no role in the design of the study; in the collection, analyses, or interpretation of data; in the writing of the manuscript; or in the decision to publish the results.

References

1. Hyder, W.; Pabani, J.K.; Luque-Nieto, M.; Laghari, A.; Otero, P. Self-Organized Ad Hoc Mobile (SOAM) Underwater Sensor Networks. *IEEE Sens. J.* **2023**, *23*, 1635–1644. [CrossRef]
2. Tian, W.; Zhao, Y.; Hou, R.; Dong, M.; Ota, K.; Zeng, D.; Zhang, J. A Centralized Control-Based Clustering Scheme for Energy Efficiency in Underwater Acoustic Sensor Networks. *IEEE Trans. Green Commun. Netw.* **2023**, *7*, 668–679. [CrossRef]
3. Yan, J.; Zhang, Z.; Yang, X.; Luo, X.; Guan, X. Target Detection in Underwater Sensor Networks by Fusion of Active and Passive Measurements. *IEEE Trans. Netw. Sci. Eng.* **2023**, *10*, 2319–2333. [CrossRef]
4. Hu, X.; Huo, Y.; Dong, X.; Wu, F.; Huang, A. Channel Prediction Using Adaptive Bidirectional GRU for Underwater MIMO Communications. *IEEE Internet Things J.* 2023. [CrossRef]

5. Su, X.; Ullah, I.; Liu, X.; Choi, D. A Review of Underwater Localization Techniques, Algorithms, and Challenges. *J. Sens.* **2020**, *2020*, 6403161. [CrossRef]
6. Sun, S.; Qin, S.; Hao, Y.; Zhang, G.; Zhao, C. Underwater Acoustic Localization of the Black Box Based on Generalized Second-Order Time Difference of Arrival (GSTDOA). *IEEE Trans. Geosci. Remote Sens.* **2020**, *99*, 1–11. [CrossRef]
7. Urazghildiiev, I.R.; Hannay, D.E. Localizing Sources Using a Network of Synchronized Compact Arrays. *IEEE J. Ocean. Eng.* **2021**, *46*, 1302–1312. [CrossRef]
8. Wang, L.; Su, D.; Liu, M.; Du, X. Modified Zeroing Neurodynamics Models for Range-Based WSN Localization from AOA and TDOA Measurements. *IEEE Sens. J.* **2022**, *22*, 13716–13726. [CrossRef]
9. Emokpae, L.E.; DiBenedetto, S.; Potteiger, B.; Younis, M.F. UREAL: Underwater Reflection-Enabled Acoustic-Based Localization. *IEEE Sens. J.* **2014**, *14*, 3915–3925. [CrossRef]
10. Ho, K.C.; Xu, W. An accurate algebraic solution for moving source location using TDOA and FDOA measurements. *IEEE Trans. Signal Process.* **2004**, *52*, 2453–2463. [CrossRef]
11. Thomson, D.J.; Dosso, S.E.; Barclay, D.R. Modeling AUV Localization Error in a Long Baseline Acoustic Positioning System. *IEEE J. Ocean. Eng.* **2018**, *43*, 955–968. [CrossRef]
12. Lei, B.; Yang, Y.; Yang, K.; Wang, Y.; Shi, Y. A hybrid passive localization method under strong interference with a preliminary experimental demonstration. *EURASIP J. Adv. Signal Process.* **2016**, *130*, 1–9. [CrossRef]
13. Zou, Y.; Liu, H.; Xie, W.; Wan, Q. Semidefinite Programming Methods for Alleviating Sensor Position Error in TDOA Localization. *IEEE Access* **2017**, *5*, 23111–23120. [CrossRef]
14. Wang, W.; Wang, G.; Zhang, F.; Li, Y. Second-Order Cone Relaxation for TDOA-Based Localization Under Mixed LOS/NLOS Conditions. *IEEE Signal Process. Lett.* **2016**, *23*, 1872–1876. [CrossRef]
15. Su, Z.; Shao, G.; Liu, H. Semidefinite Programming for NLOS Error Mitigation in TDOA Localization. *IEEE Commun. Lett.* **2018**, *22*, 1430–1433. [CrossRef]
16. Hara, S.; Anzai, D.; Yabu, T.; Lee, K.; Derham, T.; Zemek, R. A Perturbation Analysis on the Performance of TOA and TDOA Localization in Mixed LOS/NLOS Environments. *IEEE Trans. Commun.* **2013**, *61*, 679–689. [CrossRef]
17. Cao, S.; Chen, X.; Zhang, X.; Chen, X. Combined Weighted Method for TDOA-Based Localization. *IEEE Trans. Instrum. Meas.* **2020**, *69*, 1962–1971. [CrossRef]
18. Wang, G.; So, A.M.; Li, Y. Robust Convex Approximation Methods for TDOA-Based Localization Under NLOS Conditions. *IEEE Trans. Signal Process.* **2016**, *64*, 3281–3296. [CrossRef]
19. Zhao, Y.; Li, Z.; Hao, B.; Shi, J. Sensor Selection for TDOA-Based Localization in Wireless Sensor Networks with Non-Line-of-Sight Condition. *IEEE Trans. Veh. Technol.* **2019**, *68*, 9935–9950. [CrossRef]
20. Cao, Y.; Shi, W.; Sun, L.; Fu, X. Frequency-Diversity-Based Underwater Acoustic Passive Localization. *IEEE Internet Things J.* **2022**, *9*, 12641–12655. [CrossRef]
21. Liu, Y.; Wang, Y.; Chen, C. Efficient Underwater Acoustical Localization Method Based on TDOA with Sensor Position Errors. *J. Mar. Sci. Eng.* **2023**, *11*, 861. [CrossRef]
22. Ullah, I.; Liu, Y.; Su, X.; Kim, P. Efficient and Accurate Target Localization in Underwater Environment. *IEEE Access.* **2019**, *7*, 101415–101426. [CrossRef]
23. Mei, X.; Han, D.; Saeed, N.; Wu, H.; Ma, T.; Xian, J. Range Difference-Based Target Localization Under Stratification Effect and NLOS Bias in UWSNs. *IEEE Wirel. Commun. Lett.* **2022**, *11*, 2080–2084. [CrossRef]
24. Diamant, R.; Tan, H.P.; Lampe, L.H. LOS and NLOS Classification for Underwater Acoustic Localization. *IEEE. Trans. Mob. Comput.* **2014**, *13*, 311–323. [CrossRef]
25. Kay, S.M. *Fundamentals of Statistical Signal Processing, Estimation Theory*; Prentice-Hall: Upper Saddle River, NJ, USA, 1993.